Available online at www.sciencedirect.com
ScienceDirect
Surface & Coatings Technology 202 (2008) 3485–3493
SURFACE & COATINGS TECHNOLOGY
www.elsevier.com/locate/surfcoat

Properties of magnetron sputtered Al–Si–N thin films with a low and high Si content

J. Musil [a,*], M. Šašek [a], P. Zeman [a], R. Čerstvý [a], D. Heřman [a], J.G. Han [b], V. Šatava [a]

[a] Department of Physics, Faculty of Applied Sciences, University of West Bohemia, Univerzitní 22, 306 14 Plzeň, Czech Republic
[b] Center for Advanced Plasma Surface Technology, SungKyunKwan University, Suwon, Republic of Korea

Received 26 September 2007; accepted in revised form 17 December 2007
Available online 23 December 2007

Abstract

The article reports on properties of Al–Si–N films with a low (≤10 at.%) and high (≥25 at.%) Si content reactively sputtered using a closed magnetic field dual magnetron system operated in ac pulse mode. The films were sputtered from a composed target (a Si plate fixed by an Al ring with inner diameter $Ø_i$=15 or 26 mm). Main attention was devoted to the investigation of a relationship between the structure of the films and their mechanical properties, thermal stability of hardness, and oxidation resistance. It was found that (1) while the films with a low (≤10 at.%) Si content are crystalline (c-(Al–Si–N)), those with a high (≥25 at.%) Si content are amorphous (a-(Al–Si–N)) when sputtered at the substrate temperature T_s=500 °C, (2) both groups of the films exhibit (i) a high hardness H=21 and 25 GPa, respectively, and high values of the oxidation resistance exceeding 1000 °C; 1100 °C (Δm=0 mg/cm^2) and 1300 °C ($\Delta m \approx 0.003$ mg/cm^2), respectively, (3) the hardness of a-(Al–Si–N) does not vary with increasing annealing temperature T_a up to 1100 °C even after 4 h, and (4) a high oxidation resistance of c-(Al–Si–N) film with a low (<10 at.%) Si content is due to the formation of a dense, nearly amorphous Al_2O_3 surface layer which is formed in reaction of free Al atoms with ambient oxygen and prevents the fast penetration of oxygen into bulk of the film. Obtained results contribute to understand the effect of Al and Si in the Al–Si–N thin film on its mechanical properties, thermal stability and oxidation resistance.

Keywords: Al–Si–N films; Structure; Mechanical properties; Thermal annealing; Oxidation resistance; Reactive magnetron sputtering

1. Introduction

Recently, it has been recognized and experimentally demonstrated that properties of nanocomposite coatings are determined not only by their structure, elemental and phase composition but also by their nano-morphology, i.e. by the size of grains and the shape of crystallites and volume fraction of the matrix [1–7]. Besides, it has been found that the nano-morphology of a film can affect not only its enhanced properties but also can result in new unique properties. These facts have stimulated a very intensive investigation of hard nc-^{T}MeN/a-Si_3N_4 nanocomposite coatings in the last decade; here ^{T}Me=Ti, V, Cr, Zr, Nb, Mo, Hf, Ta, W, ^{T}MeN is the transition metal nitride, nc- and a- denotes the nanocrystalline and amorphous phase, respectively. Main attention in the field of hard nanocomposite coatings has been concentrated on three problems: (1) the finding of the relationship between the mechanical properties (hardness H, Young's modulus E and elastic recovery W_e), the structure, the phase composition and the nano-morphology, (2) the explanation of the origin of enhanced hardness and (3) the preparation of nanocomposites with maximum hardness H_{max} approaching or even exceeding that of the diamond. The development in this field has been established mainly by the investigation of the third problem. It has been found that the maximum hardness H_{max} is achieved in films with a low (≤10 at.%) Si content when ^{T}MeN grains are surrounded by a-Si_3N_4 tissue phase with thickness of approximately of ~1 to 2 monolayers [8]. The nitride-based nanocomposites of the type nc-^{T}MeN/a-Si_3N_4 with a low (≤10 at.%) Si content are, however, a specific group of nanocomposites exhibiting only some enhanced properties, for instance, the enhanced hardness.

* Corresponding author. Tel.: +420 377 63 22 00; fax: +420 377 63 22 02.
E-mail address: musil@kfy.zcu.cz (J. Musil).

0257-8972/$ - see front matter © 2008 Published by Elsevier B.V.
doi:10.1016/j.surfcoat.2007.12.024

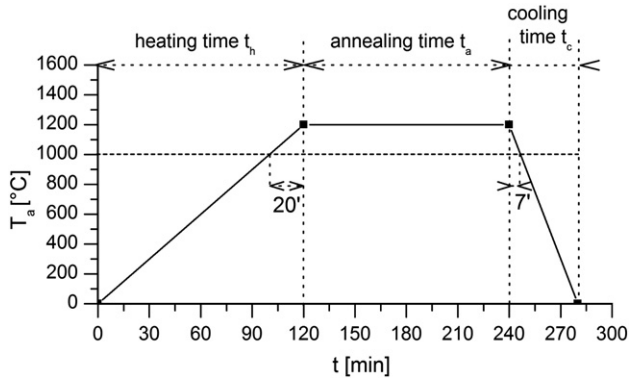

Fig. 1. Schematic diagram of three-step thermal treatment cycle. The cycle without annealing at T_a is called two-step thermal treatment cycle.

However, not only high hardness but also the thermal stability and oxidation resistance of nanocomposites at temperatures above 1000 °C is very important for new advanced applications. The nc-^{T}MeN/a-Si_3N_4 nanocomposites do not meet this requirement due to a low content of the amorphous a-Si_3N_4 phase. Therefore, the nanocomposites have been started to be doped with selected elements such as Al, Y, etc with aim to increase their thermal stability. It has been found that, for instance, the doping of TiN with Al significantly improves its oxidation resistance from ~600 to 850 °C [9]. The thermal stability and oxidation resistance of nc-^{T}MeN/a-Si_3N_4 nanocomposites with a low (≤10 at.%) Si content is limited by a low (<1000 °C) crystallization temperature of the dominating ^{T}MeN phase. Recently, it has been found that the thermal stability and oxidation resistance of the nc-^{T}MeN/a-Si_3N_4 nanocomposites can be easily increased above 1000 °C if these nanocomposites contain a high (≥25 at.%) amount of Si [10–19]. This improvement in thermal stability and oxidation resistance of nc-^{T}MeN/a-Si_3N_4 nanocomposites with a high (>20 at.%) Si content is due to their X-ray amorphous structure which remains stable during thermal annealing up to ~1400 to 1500 °C.

It is expected that similar properties should be achieved also for Al–Si–N thin films. No detailed investigation of the Al–Si–N system has been carried out so far. To our knowledge, only Ti–Si–Al–N [20–22], Ti–Al–V–Si–N [21], Ti–Cr–Al–Si–N [23] nitride thin films with a low (≤10 at.%) Si content have been investigated so far. These systems, however, also do not exhibit the thermal stability and oxidation resistance above 1000 °C because a low amount of Si prevents the formation of amorphous Al–Si based materials [24]. This fact clearly indicates that to understand the role of Al in the film, a simple Al–Si–N system with a high (≥25 at.%) Si content should be investigated at first. Recently, Patscheider et al. [25] has also reported on the investigation of the microstructure and mechanical properties of Al–Si–N coatings with Si ranging in a wide interval from 0 to 23 at.%. The aim of their study was to prepare hard, optically transparent coatings with a hardness exceeding that of Al_2O_3. No thermal stability of mechanical properties and oxidation resistance has been reported.

This article reports on a systematic investigation of the structure, mechanical properties, thermal stability and oxidation resistance of Al–Si–N films with a low (~5 at.%) and high (~40 at.%) Si content with aim to develop new hard coatings with a hardness above 20 GPa and oxidation resistance above 1000 °C.

2. Experimental

Al–Si–N films were reactively sputtered in an Ar+N_2 mixture using a closed magnetic field dual magnetron system operated in ac pulse mode generated by a pulse power supply DORA MSS-10 with output power 10 kW (produced in Poland). The repetition frequency f_r of pulses was 2 kHz and the ac frequency inside pulses was 56 kHz. The constant magnetron discharge current I_d was controlled by the duty cycle of 2 kHz pulses which ranged between 15–25% depending on the plasma impedance. Both magnetrons were equipped with the same targets (Ø 50 mm) composed of a Si plate (Ø 28 mm) fixed by an Al ring with inner diameter $Ø_i$=15 or 26 mm. The inner diameter $Ø_i$ controlled the amount of Si in the film: ~5 at.% Si at $Ø_i$=15 mm and ~40 at.% Si at $Ø_i$=26 mm. The Al–Si–N films were prepared under the following conditions: discharge current I_d=1 A, substrate bias $U_s=U_{fl}$, substrate temperature T_s=500 °C, substrate-to-target distance $d_{s\text{-}t}$=100 mm, partial pressure of nitrogen p_{N2} ranging from 0 to 0.5 Pa and total pressure $p_T=p_{Ar}+p_{N2}$=0.7 Pa; here U_{fl} is the floating potential.

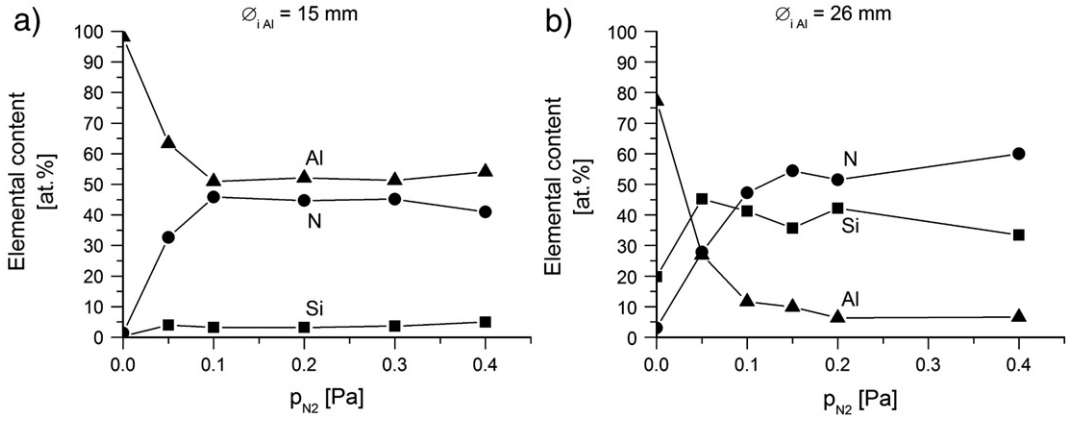

Fig. 2. Elemental composition of the Al–Si–N film with (a) a low (<10 at.%) and (b) high (~40 at.%) Si content as a function of p_{N_2}.

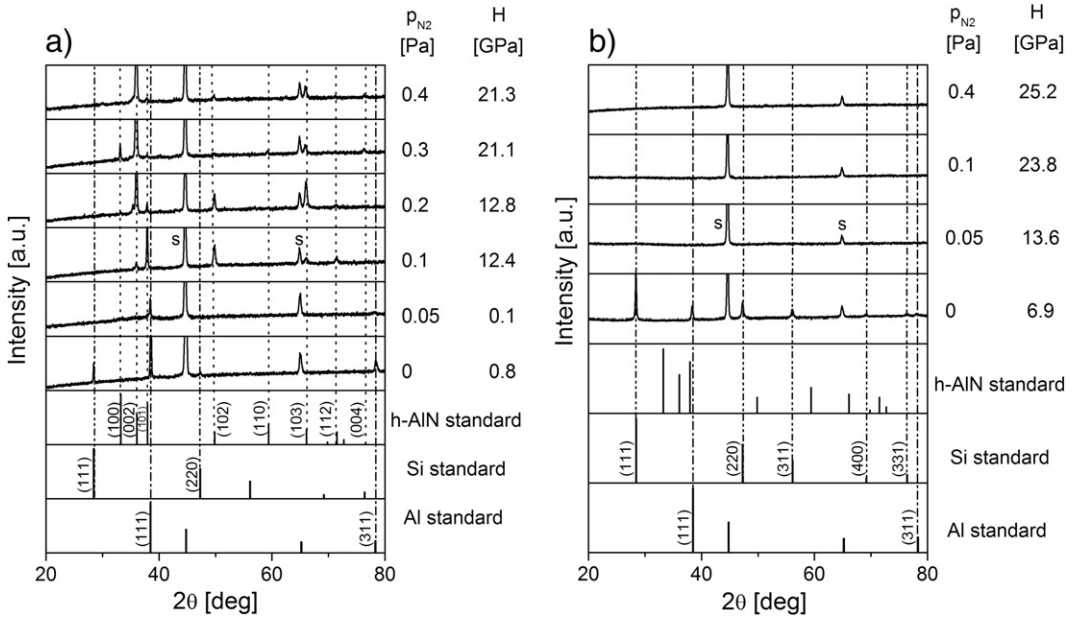

Fig. 3. Evolution of the structure of the Al–Si–N films with (a) a low (<10 at.%) and (b) high (~40 at.%) Si content sputtered on the 15330 steel with increasing p_{N_2} at T_s=500 °C, U_s=U_{fl} and p_T=0.7 Pa.

The Al–Si–N films were deposited onto CSN 15330 steel discs (Ø 25 mm, 5 mm thick), Si(111) wafers (30×5×0.4 mm^3) and sintered polycrystalline Al_2O_3 (corundum, 10×10×0.5 mm^3). The thickness h of the sputtered films ranged from ~2000 to ~5000 nm.

The film thickness and the macrostress σ were measured on films deposited on Si(111) substrates using a stylus profilometer DEKTAK 8. The macrostress σ was determined from the difference in the Si plate curvature before and after the film deposition using a Stoney's formula [26]. The film structure was characterized using an XRD spectrometer PANalytical X'Pert PRO in Bragg–Brentano configuration with CuKα radiation. The elemental composition was determined by X-Ray Fluorescence (XRF) spectroscopy with a PANalytical XRF Spectrometer MagiX PRO with the accuracy of 10% and by Rutherford back-scattering spectrometry (RBS) with the accuracy of 5%. The microstructure was characterized by a high-resolution transmission electron microscope (HRTEM) JEOL JEM-3010. Mechanical properties were determined from load vs. displacement curves measured by a microhardness tester Fischerscope H100 with a Vicker's diamond indenter at load L=50 mN. The oxidation resistance was measured in flowing air (1 l/h) using a symmetrical high-resolution Setaram thermogravimetric system TAG 2400. An annealing cycle consists generally of three steps: (1) heating from RT to a predetermined annealing temperature T_a, sometimes called the heating ramp, (2) annealing at a selected value of T_a and (3) cooling from T_a down to RT, sometimes called the cooling

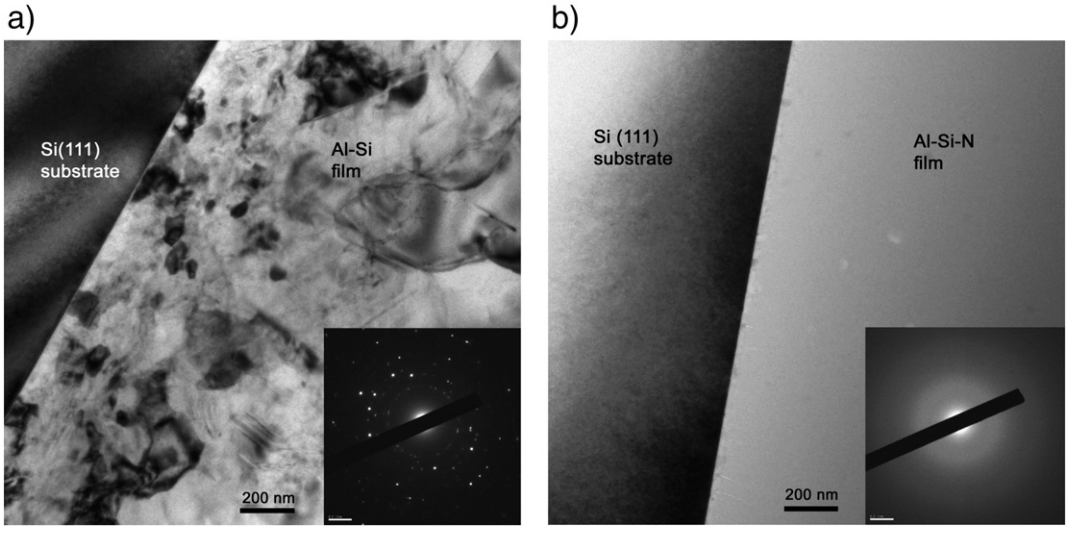

Fig. 4. Cross-section bright-field TEM images of (a) Al–Si and (b) Al–Si–N film sputtered at I_d=1 A, T_s=500 °C, p_{N_2}=0 and 0.1 Pa, respectively, on the Si(111) substrate. The electron diffraction patterns are inserted.

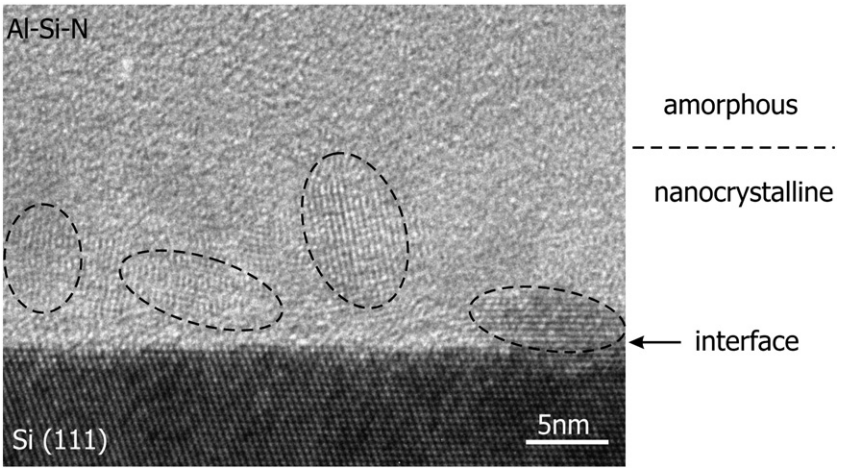

Fig. 5. Bright-field image of the interface region in the cross-section of a Al–Si–N film sputtered at I_d=1 A, T_s=500 °C, p_{N_2}=0.1 Pa and p_T=0.7 Pa (Fig. 4b).

ramp, see Fig. 1. In some experiments, annealing at T_a is omitted, i.e. the temperature is increased to T_a and immediately decreased down to RT. Such thermal annealing is called *two-step thermal treatment cycle*. Thermal annealing experiments were carried out at 10 °C/min heating and 30 °C/min cooling rate, respectively, on substrates coated only on one side. Thermogravimetric curves corresponding to oxidation of the bare substrates were subsequently subtracted and the resulting curves then characterized the oxidation resistance of pure films only, without any substrate effects. The measurements of all the parameters of sputtered Al–Si–N films were performed with an accuracy better than 10%.

3. Results and discussion

3.1. Elemental composition

The elemental composition of the Al–Si–N films is strongly influenced by the partial pressure of nitrogen p_{N2} and the inner diameter $Ø_i$ of the Al fixing ring, see Fig. 2. The amount of Si in the film is low (~5 at.%) when Al ring with $Ø_i$=15 mm is used (Fig. 2a). From this figure it is clearly seen that (i) in the Al–Si–N films with a low Si content Al dominates over Si for all p_{N2} used and (ii) the Al–Si–N films sputtered at $p_{N_2} \geq 0.1$ Pa exhibit almost the same elemental composition. Based on known values of the formation enthalpies, $\Delta H_{Si_3N4} = -745.1$ kJ/mol and $\Delta H_{AlN} = -318.6$ kJ/mol [27], we assume that N has a higher affinity to Si than to Al and thus the Si_3N_4 phase is formed at first. Because the amount of N is lower than that necessary for the formation of stoichiometric Si_3N_4 and AlN the films should be composed of a mixture of Si_3N_4+AlN+Al. It means that all the sputtered Al–Si–N films with a low Si content contain free Al atoms. Free Al atoms can be easily oxidized resulting in an enhancement of the oxidation resistance; details are given in Section 3.6.2. The amount of Si in the film is high (~40 at.%) when the Al ring with $Ø_i$=26 mm is used (Fig. 2b). In this case the amount of N is higher than that of Si and Al at $p_{N_2} > 0.1$ Pa and no free Al is expected to be in Al–Si–N films produced at $p_{N_2} > 0.1$ Pa.

3.2. Structure

The developments of the structure of the Al–Si–N films with a low (<10 at.%) and high (~40 at.%) Si content with increasing p_{N2} are shown in Fig. 3.

3.2.1. Al–Si–N films with a low (<10 at.%) Si content

All the films are crystalline. The Al–Si film sputtered at p_{N_2}=0 Pa is polycrystalline with strong Al(111) and weak Al (311), Si(111) and Si(220) X-ray reflections. The low-intensity Si reflections correspond to a low amount of Si in the film. Already a small addition of N_2 to Ar gas leads to a considerable increase (~30 at.%) of N in the film resulting in a strong suppression of Si and Al reflections and in the formation of hexagonal AlN grains, which change the preferred crystallographic orientation from (101) to (002) with increasing p_{N_2}. The Al–Si–N films with no Al(111) reflection produced at $p_{N_2} \geq 0.3$ Pa exhibit the highest hardness $H \approx 21$ GPa.

3.2.2. Al–Si–N films with a high (~40 at.%) Si content

The films are characterized with a polycrystalline Al–Si structure for p_{N_2}=0 Pa and an X-ray amorphous Al–Si–N structure for $p_{N_2} > 0$ Pa on polycrystalline 15330 steel. From Fig. 3 it is clearly seen that already a very small addition of

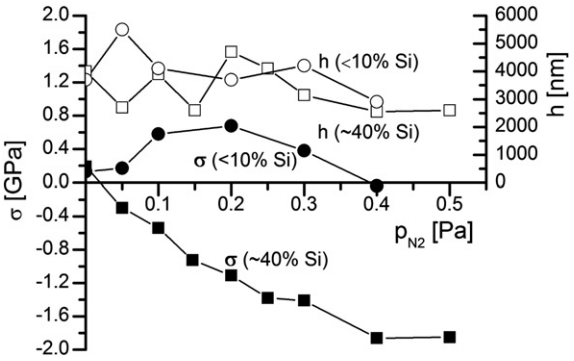

Fig. 6. Macrostress σ in the Al–Si–N films and their thickness *h* as a function of p_{N_2}.

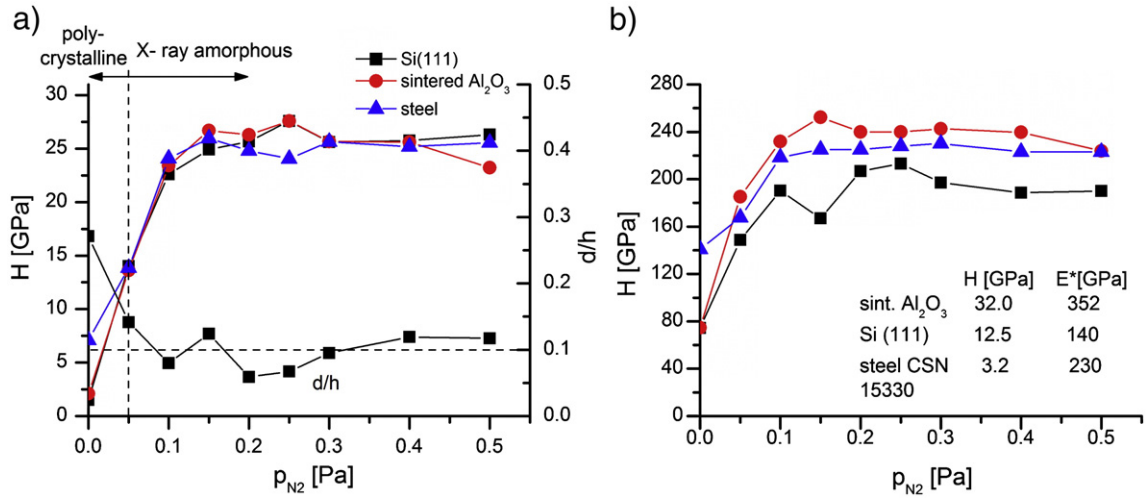

Fig. 7. Developments of (a) hardness H and (b) effective Young's modulus E^* of the Al–Si–N films with a high (~40 at.%) Si content, sputtered on Si(111), steel and sintered Al_2O_3 substrates, with increasing partial pressure of nitrogen p_{N_2}. The ratio d/h in Fig. 7a shows a correctness of the H measurement; d is the indentation depth of diamond indenter and h is the film thickness.

nitrogen (p_{N_2}=0.05 Pa) is sufficient to create the X-ray amorphous Al–Si–N film in spite of the fact that the substrate temperature T_s=500 °C, used in sputtering, is relatively high.

3.3. Microstructure

The microstructure of Al–Si and Al–Si–N films with a high (~40 at.%) Si content was characterized using bright-field TEM images. The images of cross-section of the Al–Si and Al–Si–N films are displayed in Fig. 4. From these images it is clearly seen that while the Al–Si film exhibits a polycrystalline structure, the Al–Si–N film is completely amorphous. This fact is confirmed by the electron diffraction patterns which are inserted in Figs. 4a and b and also by XRD patterns displayed in Fig. 3b.

In spite of the amorphous structure of the Al–Si–N film sputtered at p_{N_2}=0.1 Pa, the film is nanocrystalline near the interface, see Fig. 5. The nanocrystalline region is very thin ~12 nm. The origin of nanocrystallization at the interface is probably due to the substrate; this phenomenon is a subject of experiments being now carried out in our labs.

3.4. Macrostress

The macrostress σ generated in the Al–Si–N films during sputtering strongly depends on both (i) the Si content in the film and (ii) the partial pressure of nitrogen p_{N_2}. This fact is shown in Fig. 6 where the dependence $\sigma=f(p_{N_2})$ in thick (~2500 nm to ~5000 nm) Al–Si–N films with a low (<10 at.%) and high (~40 at.%) Si content is displayed.

The Al–Si–N films with a low (<10 at.%) Si content exhibit a tensile stress $\sigma>0$. On the contrary, the Al–Si–N films with a high (~40 at.%) Si content is in compression stress ($\sigma<0$). The measurement of the elemental composition of the Al–Si–N films produced at different values of p_{N_2} indicates that the increase in compressive stress σ correlates well with the increase of the amount N in the films. Because the formation enthalpy ΔH_f of Si_3N_4 (−745.1 kJ/mol [27]) is higher than that of AlN (−318.6 kJ/mol [27]), the Si_3N_4 phase, which is amorphous (a-Si_3N_4) due to a low deposition temperature (T_s=500 °C), is formed at first. The aluminum nitride AlN starts to form at p_{N_2} when all Si is converted into a-Si_3N_4. We believe

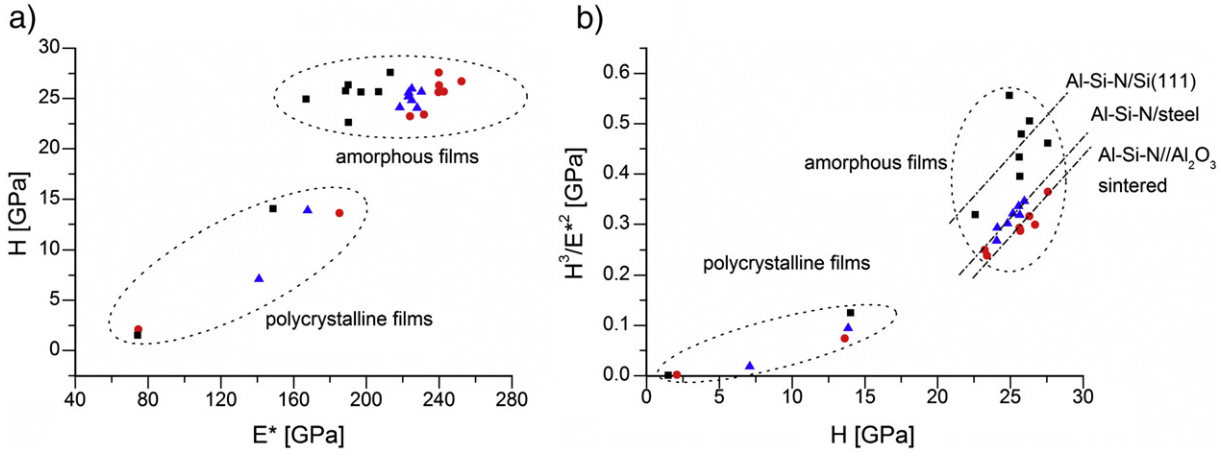

Fig. 8. $H=f(E^*)$ and $H^3/E^{*2}=f(H)$ for the Al–Si–N films with a high (~40 at.%) Si content sputtered on Si(111), steel and sintered Al_2O_3 substrates.

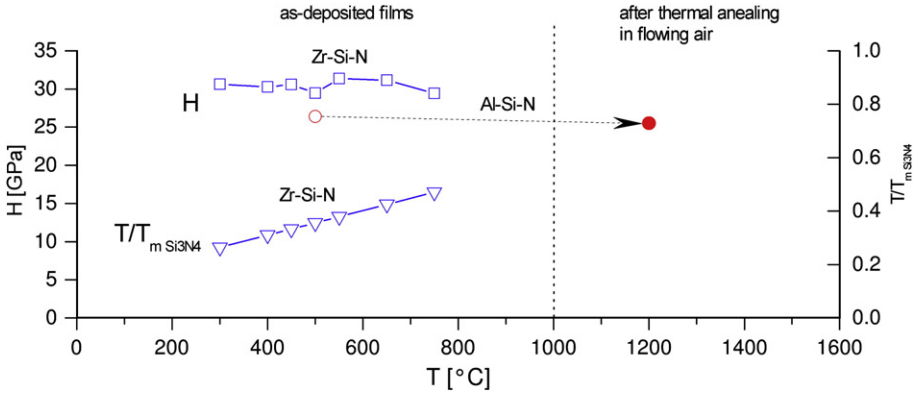

Fig. 9. Hardness H of as-deposited Zr–Si–N films with a high (>20 at.%) Si content sputtered at I_d=1 A, p_{N_2}=0.4 Pa and different values of T_s on the Si(100) substrate and the Al–Si–N film with a high (~40 at.%) Si content sputtered at p_{N_2}=0.4 Pa and T_s=500 °C after its thermal annealing in two-step cycle in flowing air.

that the increase in compressive stress σ is connected with the formation of nitride phases in the Al–Si–N composite films, particularly with an incorporation of AlN grains into an amorphous a-Si_3N_4 matrix. In spite of the increase of the compressive stress σ with increasing p_{N_2}, its saturation value is relatively low, of about −1.8 GPa in the ~3000 nm thick Al–Si–N film. A similar value $\sigma_{max} \approx -1.5$ GPa has been recently measured also for Ti–Si–N films with a high Si content [17].

3.5. Mechanical properties

Basic mechanical properties of materials are (i) hardness H, (ii) effective Young's modulus $E^* = E/(1-\nu^2)$, and (iii) resistance to plastic deformation directly proportional to the ratio H^3/E^{*2} [28]; here E is the Young's modulus and ν is the Poisson's ratio.

In this paper, the mechanical properties of the Al–Si–N films with a high (~40 at.%) Si content are discussed only; for the mechanical properties of the films with a low Si content see, for instance, Ref. [25]. The films were sputtered on Si (111), 15330 steel and sintered Al_2O_3 substrates. The hardness H and effective Young's modulus E^* as a function of p_{N_2} are displayed in Fig. 7. Both H and E^* strongly increase with increasing p_{N_2} up to ~0.1 Pa. The Al–Si–N films sputtered at p_{N_2}>0.1 Pa exhibit almost the same value of $H \approx 25$ GPa. This is a maximum value of H_{max} of the Al–Si–N films sputtered under conditions given in Section 2. It is also necessary to note that the maximum value of H_{max} practically does not depend on the substrate. On the contrary, maximum values of the Young's modulus E^*_f of the Al–Si–N films strongly depend on the substrate. The higher the effective Young's modulus E^*_s of the substrate is, the higher the maximum value of $E^*_{f\,max}$ of the Al–Si–N film is.

The mechanical behavior of materials is determined by a combined action of hardness H and Young's modulus E^* [29–31]. Therefore, it is important to know the interrelationship between H and E^* and the relation between the ratio H^3/E^{*2} and H, see Fig. 8. Three issues can be drawn from Fig. 8a: (1) H approximately increases with increasing E^*, (2) the polycrystalline c-(Al–Si–N) films exhibit a lower hardness ($H \leq 15$ GPa) and (3) the amorphous a-(Al–Si–N) films with almost the same hardness exhibit the lower value of Young's modulus E^*_f in the case when the Young's modulus of the substrate E^*_s is lower; the last fact is also seen in Fig. 7b. Fig. 8b clearly shows that a-

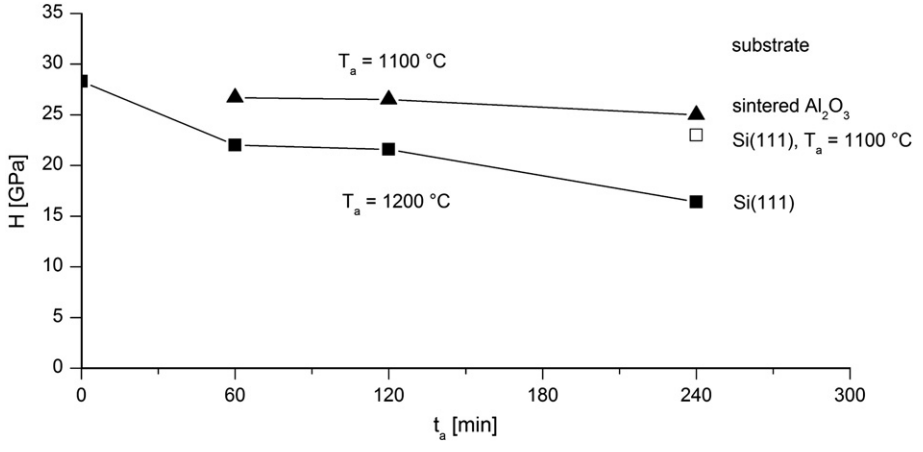

Fig. 10. Variation of hardness H of a 2500 nm thick $Si_{33}Al_7N_{60}$ film sputtered on the Si (111) and sintered Al_2O_3 substrates with increasing annealing time t_a in three-step thermal treatment process at two values of T_a=1100 °C and 1200 °C.

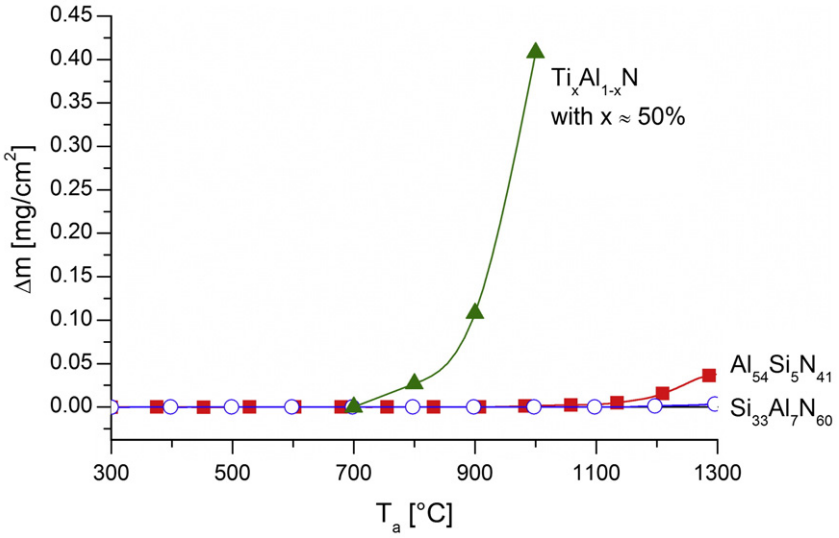

Fig. 11. Mass increase Δm of ~2500 nm thick (a) polycrystalline $Al_{54}Si_5N_{41}$ and (b) amorphous $Si_{33}Al_7N_{60}$ films, sputtered on the Si(111) and Al_2O_3 substrates, as a function of annealing temperature T_a in two-step thermal treatment process with 10 °C/min heating and 30 °C/min cooling rate, respectively.

(Al–Si–N) films exhibit a higher resistance to plastic deformation (a higher ratio H^3/E^{*2}).

3.6. Thermal stability

The thermal stability of mechanical and physical properties is of a key importance for every thin film and coating. The thermal stability is defined as a temperature T_{stab} at which the mechanical properties of the coating start to change. The temperature T_{ox} at which the coating starts to oxidize is called the oxidation resistance of the coating. Experiments performed so far indicate that $T_{ox} \approx T_{stab}$.

3.6.1. Thermal stability of hardness

The measurement of the thermal stability of hardness H of sputtered films can be realized by two methods: (1) by increasing of the substrate temperature T_s, and (2) by thermal annealing of as-deposited films in air. As an example of the first method, the hardness H of amorphous Zr–Si–N films with a high (≥ 50 vol. %) content of the Si_3N_4 phase deposited at different values of T_s is displayed in Fig. 9; for more details see Refs. [13,16]. From this figure it is seen that H almost does not depend on T_s. It indicates that H is determined by the amorphous structure of the film and not by the macrostress σ generated in the film during its growth. Namely, if H is determined by σ, its value should decrease with increasing value of T_s because the ratio $T_s/T_m > 0.2$ increases with increasing T_s and already the ratio $T_s/T_m \approx 0.25$ should be sufficient to relax the macrostress σ in nitride films [32]. The amorphous a-(Al–Si–N) films with a high (~40 at.%) Si content sputtered at $T_s = 500$ °C also exhibit a high (>0.3) ratio T_s/T_m; $T_{m\ Si_3N4} = 2173$ K, $T_{m\ AlN} = 2523$ K [33] and $T_s/T_m > 0.3$ for both the Si_3N_4 and AlN phases under the assumption that exist separately in the Al–Si–N thin film. Therefore, no dependence $H = f(T_s)$ was investigated for the amorphous a-(Al–Si–N) films with a high Si content.

The effect of the post-deposition annealing on the film hardness H was tested on the a-(Al–Si–N) film with a high (~40 at.%) Si content. The post-deposition annealing of the Al–Si–N film sputtered at $T_s = 500$ °C in two-step thermal treatment cycle with a maximum annealing temperature 1200 °C (the temperature in this process was above 1000 °C for 27 min) does not influence its hardness H because of a perfect thermal stability of the amorphous structure of the film at $T_a \leq 1200$ °C. Practically no decrease in H was measured after the thermal treatment process, see Fig. 9. Also, no change in the X-ray amorphous structure was found. It means that the thermal stability of the amorphous structure also results in the thermal stability of the mechanical properties.

3.6.1.1. Effect of annealing time. The film properties can be influenced not only by the value of T_a but also by the annealing time t_a at a given temperature T_a. The dependence of H of the Al–Si–N film, sputtered on Si(111) and Al_2O_3 substrate, as a function t_a at two values of $T_a = 1100$ °C and 1200 °C (three-step thermal treatment cycle) is displayed in Fig. 10. The hardness H of the Al–Si–N film on both Si(111) and Al_2O_3

Table 1
Mechanical properties of the Al–Si–N films with a low and high Si content used in the oxidation experiments

Film	h [nm]	Al	Si [at. %]	N	H [GPa]	E^* [GPa]	H^3/E^{*2} [GPa]	σ [GPa]	a_D [nm/min]	Structure
$Al_{54}Si_5N_{41}$	2600	54	5	41	21.3	230	0.18	−0.04	6.2	Crystalline
$Si_{33}Al_7N_{60}$	2500	7	33	60	25.6	240	0.29	−1.8	10.6	Amorphous

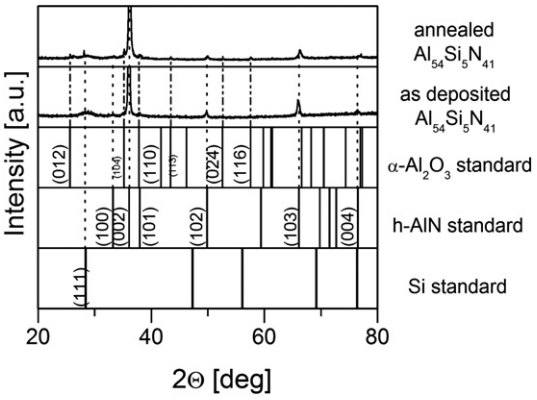

Fig. 12. XRD patterns from c-$Al_{54}Si_5N_{41}$/Si(111) in the as-deposited state and after thermal annealing in two-step cycle up to 1300 °C in flowing air at a 10 °C/min heating and 30 °C/min cooling rate, respectively.

substrates remains almost constant during annealing at T_a=1100 °C for t_a=4 h. When T_a is increased to 1200 °C, the hardness H of the film deposited on the Si(111) substrate continuously decreases with increasing annealing time from ~27 GPa to ~17 GPa. That is probably caused by a slight oxidation of the film which results in the formation of a surface oxide layer growing in the thickness with the annealing time t_a and having a lower hardness than the Al–Si–N film bulk; for more details see Ref. [14] where a similar phenomenon has been investigated. The dependence $H=f(t_a)$ of Al–Si–N films sputtered on the Al_2O_3 substrate has not been investigated so far.

3.6.2. Oxidation resistance

Generally, the oxidation resistance of a film strongly depends on its structure. Recently, it has been found that hard amorphous ^{T}Me–Si–N films with a high (>20 at.%) Si content exhibit better oxidation resistance compared to polycrystalline ones [6,7,18,19]. Experiments described in this paper, however, show that the Al–Si–N films, in which ^{T}Me was replaced with Al, also exhibit a high oxidation resistance, see Fig. 11. In this figure the oxidation resistance of the Al–Si–N films with a low (5 at.%) and high (33 at.%) Si content, i.e. $Al_{54}Si_5N_{41}$ and $Si_{33}Al_7N_{60}$ films, is compared. The mechanical properties of the as-deposited Al–Si–N films used in the oxidation experiment are summarized in Table 1. The crystalline c-(Al–Si–N) film exhibits a high oxidation resistance up to ~1000 °C (an increase in mass Δm<0.005 mg/cm^2 in two-step thermal treatment process when the film is deposited on the Si(111) substrate) and the amorphous a-(Al–Si–N) film exhibits even higher oxidation resistance, up to ~1150 °C (Δm=0 in two-step thermal treatment process when the film is deposited on the Al_2O_3 substrate).

This experiment clearly shows that the crystalline Al–Si–N films containing a large amount of Al also exhibit a good oxidation resistance. That is due to the existence of free Al atoms in the film, their easy oxidation and the formation of a dense Al_2O_3 surface layer preventing the fast penetration of oxygen into the bulk of the film.

3.6.2.1. Structure of thermally annealed Al–Si–N films. The structure of the Al–Si–N films with both a low (5 at.%) and high (33 at.%) Si content practically does not change during thermal annealing in two-step treatment process up to 1300 °C. The amorphous structure of the as-deposited $Si_{33}Al_7N_{60}$ film remains amorphous and the as-deposited $Al_{54}Si_5N_{41}$ film with hexagonal AlN(002) preferred crystallographic orientation remains crystalline with the same preferred orientation, see Fig. 12. After the annealing the $Al_{54}Si_5N_{41}$ film also exhibits low-intensity Al_2O_3(012), (104), (110) and (116) reflections.

3.6.2.2. Comparison of oxidation resistance of Al–Si–N film with ^{T}Me–Si–N films. Recently, an excellent oxidation resistance of amorphous ^{T}Me–Si–N films considerably exceeding 1000 °C has been reported [5–7,10–19]. Experiments described in this paper show that the replacement of ^{T}Me with Al in ^{T}Me–Si–N films with a high (>20 at.%) Si content also results in an excellent oxidation resistance of Al–Si–N films, see Fig. 13. A low (~800 °C) oxidation of the $Si_{24}W_{17}N_{59}$ film is due to the formation of volatile oxides [13]. In Fig. 13 the oxidation resistance of a polycrystalline TiAlN film [9] is also given for a comparison.

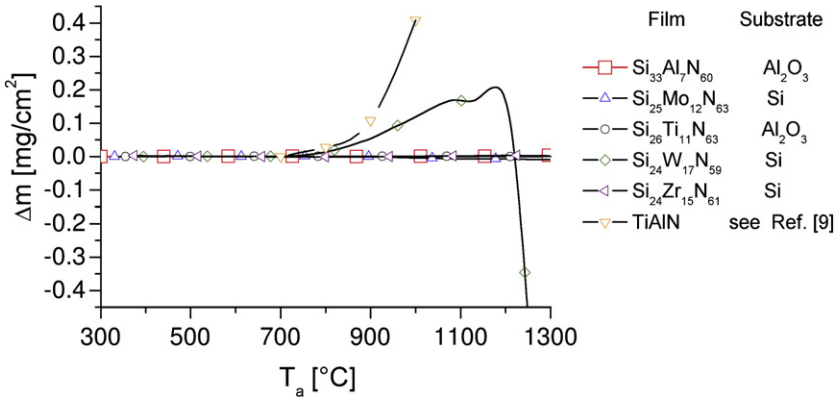

Fig. 13. Comparison of the oxidation resistance of a ~2600 nm thick amorphous $Si_{33}Al_7N_{60}$ film with selected (i) ^{T}Me–Si–N films with a high (>20 at.%) Si content and (ii) TiAlN film [9], represented by an increase in the film mass Δm as a function of T_a.

4. Conclusions

Main results of the investigation of the sputtered Al–Si–N films are the following:

1. The Al–Si–N films with a low (<10 at.%) Si content are polycrystalline. On the contrary, the Al–Si–N films with a high (≥20 at.%) Si content are amorphous in spite of the fact that they are sputtered at relatively high values of the substrate temperature T_s=500 °C.
2. The amorphous a-(Al–Si–N) films are (i) harder and (ii) more resistant to plastic deformation compared to the polycrystalline c-(Al–Si–N) films.
3. The thermal stability of hardness H of the a-(Al–Si–N) film is high and does not vary with increasing annealing temperature T_a up to 1100 °C even after 4 h.
4. The oxidation resistance of both the crystalline c-(Al–Si–N) film with a low (<10 at.%) Si content and the amorphous a-(Al–Si–N) film with a high (≥20 at.%) Si content is also high. The c-(Al–Si–N) film exhibits a high oxidation resistance up to ~1000 °C and the a-(Al–Si–N) film up to ~1150 °C.
5. A high oxidation resistance of the c-(Al–Si–N) film with a low (<10 at.%) Si content is due to the existence of free Al atoms in the film, their easy oxidation and the formation of a dense Al_2O_3 surface layer which prevents a fast penetration of the oxygen into bulk of the film.

Obtained results indicate that the substitution of ^{T}Me with Al in ^{T}Me–Si–N films results in the formation of hard Al–Si–N films with good and thermally stable mechanical properties and excellent oxidation resistance exceeding 1000 °C.

Acknowledgements

This work was supported in part by the Ministry of Education of the Czech Republic under Project Nos. MSM 4977751302 and ME 673, and the Grant Agency of the Czech Republic under project No. 106/06/0327.

References

[1] H. Gleiter, Prog. Mater. Sci. 33 (1989) 223.
[2] S. Veprek, J. Vac. Sci. Technol. A17 (1999) 2401.
[3] J. Musil, Surf. Coat. Technol. 125 (2000) 322.
[4] J. Patscheider, MRS Bull. 28 (3) (2003) 180.
[5] J. Musil, in: J.Th.M. De Hosson, A. Cavaleiro (Eds.), Nanostructured Hard Coatings, Kluwer Academic/Plenum Publishers, New York, USA, 2006, p. 407.
[6] J. Musil, in: S. Zhang, N. Ali (Eds.), Nanocomposite films and coatings, Imperial College Press, London, UK, 2007, p. 281.
[7] J. Musil, P. Baroch, P. Zeman: in R. Wei (Ed.), Plasma Surface Engineering and its Practical Applications, Research Signpost Publisher, USA, in press.
[8] S. Veprek, S. Reiprich, Thin Solid Films 268 (1995) 64.
[9] W.-D. Münz, J. Vac. Sci. Technol. A4 (1986) 2717.
[10] H. Zeman, J. Musil, P. Zeman, J. Vac. Sci. Technol. A22 (2004) 646.
[11] J. Musil, R. Daniel, P. Zeman, O. Takai, Thin Solid Films 478 (2005) 238.
[12] J. Musil, P. Dohnal, P. Zeman, J. Vac. Sci. Technol. B23 (2005) 1568.
[13] J. Musil, R. Daniel, J. Soldan, P. Zeman, Surf. Coat. Technol. 200 (2006) 3886.
[14] P. Zeman, J. Musil, R. Daniel, Surf. Coat. Technol. 200 (2006) 4091.
[15] P. Zeman, J. Musil, Appl. Surf. Sci. 252 (2006) 8319.
[16] R. Daniel, J. Musil, P. Zeman, C. Mitterer, Surf. Coat. Technol. 201 (2006) 3368.
[17] J. Musil, P. Zeman, P. Dohnal, R. Čerstvý, Plasma Process. Polym. 4 (2007) S574.
[18] J. Musil, P. Zeman, Solid State Phenomena 127 (2007) 31.
[19] J. Musil, J. Vlcek, P. Zeman, Advanced amorphous non-oxide coatings with oxidation resistance above 1000 °C, Advances in Applied Ceramics, Special Issue on NANOCERAMICS, submitted for publication.
[20] S. Carvalho, L. Rebouta, A. Cavaleiro, L.A. Rocha, J. Gomes, E. Alves, Thin Solid Films 398-399 (2001) 391.
[21] P.J. Martin, A. Bendavid, J.M. Cairney, M. Hoffman, Surf. Coat. Technol. 200 (2005) 2228.
[22] S. Carvalho, E. Ribeiro, L. Rebouta, C. Tavares, J.P. Mendoca, A.C. Monteiro, N.J.M. Carvalho, J.Th.M. De Hosson, A. Cavaleiro, Surf. Coat. Technol. 177-178 (2004) 459.
[23] K. Yamamoto, S. Kujime, K. Takahara, Surf. Coat. Technol. 200 (2005) 1383.
[24] M. Naka, T. Shibayanagi, M. Maeda, S. Zhao, H. Mori, Vacuum 59 (2000) 252.
[25] A. Pelisson, M. Parlinska-Wojtan, H.J. Hug, J. Patscheider, Surf. Coat. Technol. 202 (2007) 884.
[26] J.D. Wilcock, D.S. Cambell, Thin Solid Films 3 (1969) 3.
[27] E.A. Brandes (Ed.), Smithells Metals Reference Book, 7th Edition, Butterworth Heinemann, 1992, pp. 8–23.
[28] T.Y. Tsui, G.M. Pharr, W.C. Oliver, et al., Mater. Res. Soc. Symp. Proc. 383 (1995) 447.
[29] J. Musil, F. Kunc, H. Zeman, H. Poláková, Surf. Coat. Technol. 154 (2002) 304.
[30] M. Jirout, J. Musil, Surf. Coat. Technol. 200 (2006) 6792.
[31] J. Musil, M. Jirout, Surf. Coat. Technol. 201 (2007) 5148.
[32] J.A. Thornton, D.W. Hoffman, Thin Solid Films 171 (1989) 5.
[33] H. Holleck, J. Vac. Sci. Technol. A4 (1986) 2662.